

# Fixed Point Properties of the Ising Ferromagnet on the Hanoi Networks

S. Boettcher\* and C. T. Brunson

*Physics Dept., Emory University, Atlanta, GA 30322; USA*

The Ising model with ferromagnetic couplings on the Hanoi networks is analyzed with an exact renormalization group. In particular, the fixed-points are determined and the renormalization-group flow for certain initial conditions is analyzed. Hanoi networks combine a one-dimensional lattice structure with a hierarchy of long-range bonds to create a mix of geometric and small-world properties. Generically, those small-world bonds result in non-universal behavior, i.e. fixed points and scaling exponents that depend on temperature and the initial choice of coupling strengths. It is shown that a diversity of different behaviors can be observed with seemingly small changes in the structure of the networks. Defining interpolating families of such networks, we find tunable transitions between regimes with power-law and certain essential singularities in the critical scaling of the correlation length. These are similar to the so-called inverted Berezinskii-Kosterlitz-Thouless transition previously observed only in scale-free or dense networks.

## I. INTRODUCTION

The study of equilibrium statistical models, in particular the Ising model, on complex networks have led to a number of novel phenomena, many of which still defy proper classification [1, 2]. The reasons for that originate with the diversity of network structures conceivable, where the most basic features, such as their degree distribution or average range of connections, are insufficient to characterize their asymptotic properties. Instead, even within a given ensemble of networks, scaling behavior may depend strongly on the details of the network structure or the strength of the interactions. Despite of that high degree of non-universality, in fact, quite different types of networks exhibit qualitatively very similar phenomena. That circumstance likely points toward the possibility of generalized classification scheme for statistical models in a networked world. We will discuss the possibilities of such a classification elsewhere [3].

One such ubiquitous phenomenon is the so-called inverted Berezinskii-Kosterlitz-Thouless transition (BKT) [2], named after the distinctly weak infinite-order BKT phase transition observed for the  $O(2)$ -vector model on a two-dimensional lattice [4–6]. In the original BKT transition, spin-waves curl into vortex structures, whose pair-creation and unbinding dominates the low-temperature behavior of the system. Renormalization group analysis demonstrates the existence of a line of stable fixed points in the low- $T$  regime that is parameterized by the temperature  $T$ , resulting in an equally  $T$ -dependent scaling behavior and an exponential singularity for the correlation length there. Analogously, for several Ising spin systems on certain networks, a similar  $T$ -dependent line of absorbing fixed points has been found, but *inverted* in the sense that it occurs only in the *high*-temperature regime, for all  $T > T_c$  [7–11]. Clearly, such a behavior can not be related to spin-waves due to the discrete,  $O(1)$ -

symmetry of Ising spins, nor to any topological defects such as vortices due to the long-range nature of bonds in any of these networks.

Here, we use an exact real-space renormalization group (RG) to study the ferromagnetic Ising model on the recently introduced set of Hanoi networks [12–14]. Hanoi networks have been used to study phenomena as diverse as diffusion [13, 14], synchronization [12], the exclusion process [15], percolation [16], quantum transport [17], and the vertex cover problem [18]. These hierarchically constructed networks possess a regular degree or have an exponential degree distribution, akin to the Watts-Strogatz Small Worlds [19]. Unlike scale-free networks often used to model social phenomena [20, 21], they have a more “physically” desirable geometry [22] of a lattice backbone mixed with a small-world hierarchy. With regard to spin models, certain Hanoi networks might combine finite transition temperatures with susceptibilities that exist in the high-temperature regime. They hold the potential for an interesting, analytically tractable interpolation from that small-world behavior toward that of a finite dimensional lattice [23, 24] by re-weighting long-range bonds. As some of those features are lacking in other hierarchical networks [8, 25–27], this will serve as focus of future investigations. For these Hanoi networks, we determine the location of stable and unstable fixed points in their phase diagrams and find a range of interesting RG-flows. Our results demonstrate that a scale-free network or highly heterogeneous coupling strengths is not a prerequisite for the BKT transition. Moreover, we provide analytically tractable one-parameter interpolations between a ferromagnetic transition governed by unstable fixed points and BKT-like transitions. In general, we find that the critical divergence of the correlation length with temperature becomes increasingly singular – from power-law over BKT-like to a full essential singularity – for increasing relative strength of long-range couplings in the network.

In the following Section, we describe the Hanoi networks. The analysis of the phase diagrams and the RG-flow for the Ising ferromagnet on these networks is discussed in Sec. III. In Sec. IV, we introduce families of

---

\*URL: <http://www.physics.emory.edu/faculty/boettcher/>

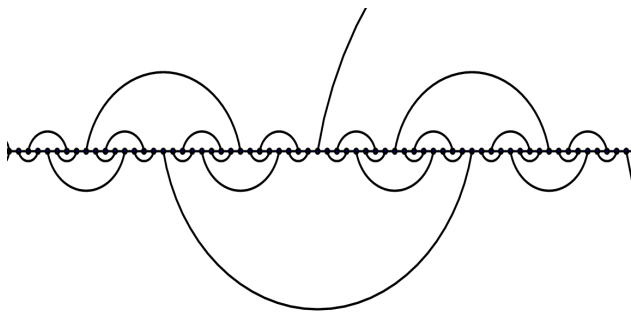


FIG. 1: (Color Online) Depiction of the 3-regular network HN3 on a semi-infinite line.

interpolating networks to reveal a more comprehensive set of regimes, each with its own characteristic type of phase transition, and we conclude with a discussion of our results in their implications in Sec. V.

## II. GEOMETRY OF THE HANOI NETWORKS

Each of the Hanoi networks possesses a simple geometric backbone, a one-dimensional line of sites  $n$ ,  $0 \leq n \leq N = 2^k$  ( $k \rightarrow \infty$ ). Each site is connected to its nearest neighbor, ensuring the existence of the  $1d$ -backbone. To generate the small-world hierarchy in these networks, consider parameterizing any integer  $n$  (except for zero) *uniquely* in terms of two other integers  $(i, j)$ ,  $i \geq 0$ , via

$$n = 2^i (2j + 1). \quad (1)$$

Here,  $i$  denotes the level in the hierarchy whereas  $j \geq 0$  labels consecutive sites within each hierarchy. For instance,  $i = 0$  refers to all odd integers,  $i = 1$  to all integers once divisible by 2 (i.e., 2, 6, 10,...), and so on. Depending on its level of the hierarchy, any site has also small-world (i.e. long-range) bonds to more-distant sites along the backbone, according to some non-random rule. For example, we obtain a 3-regular network HN3 by connecting also 1 to 3, 5 to 7, 9 to 11, etc, for  $i = 0$ , next 2 to 6, 10 to 14, etc, for  $i = 1$ , and 4 to 12, 20 to 28, etc., for  $i = 2$ , and so on, as depicted in Fig. 1.

Previously[12], it was found that the average chemical path between sites on HN3 scales as

$$d^{HN3} \sim \sqrt{l} \quad (2)$$

with the distance  $l$  along the backbone. In some ways, this property is reminiscent of a square-lattice consisting of  $N$  lattice sites. The diameter (=diagonal) of this square is also  $\sim \sqrt{N}$ .

While HN3 (and HN4 [12]) are of a fixed, finite degree, we introduced here convenient generalizations of HN3 that lead to new, revealing insights into small-world phenomena. First, we can extend HN3 in the following manner to obtain a new planar network of average degree

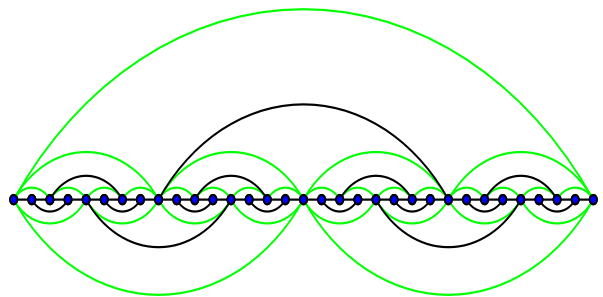


FIG. 2: (Color Online) Depiction of the planar network HN5, comprised of HN3 (black lines) with the addition of further long-range bonds (green-shaded lines). Note that sites on the lowest level of the hierarchy have degree 3, then degree 5, 7, etc, comprising a fraction of  $1/2$ ,  $1/4$ ,  $1/8$ , etc., of all sites, which makes for an average degree 5 in this network.

5, hence called HN5: In addition to the bonds in HN3, in HN5 we also connect all even sites to both nearest sites *within* the same level of the hierarchy  $i (\geq 1)$ . The resulting network remains planar but now sites have a hierarchy-dependent degree, as shown in Fig. 2. To obtain the average degree, we observe that  $1/2$  of all sites have degree 3,  $1/4$  has degree 5,  $1/8$  has degree 7, and so on, leading to an exponentially falling degree distribution of  $\mathcal{P}\{\alpha = 2i + 3\} \propto 2^{-i}$ . Then, the total number of bonds  $L$  in the system of size  $N = 2^k$  is

$$\begin{aligned} 2L &= 2(2k - 1) + \sum_{i=0}^{k-2} (2i + 3) 2^{k-1-i} \\ &= 5 \times 2^k - 8, \end{aligned} \quad (3)$$

and thus, the average degree is

$$\langle \alpha \rangle = \frac{2L}{N} \sim 5. \quad (4)$$

In HN5, the end-to-end distance is trivially 1, see Fig. 2. Therefore, we define as the diameter the largest of the shortest paths possible between any two sites, which are typically odd-index sites furthest away from long-distance bonds. For the  $N = 32$  site network depicted in Fig. 2, for instance, that diameter is 5, measured between site 3 and 19 (starting with  $n = 0$  as the left-most site), although there are many other such pairs. It is easy to show recursively that this diameter grows as

$$d^{HN5} = 2 \left\lfloor \frac{k}{2} \right\rfloor + 1 \sim \log_2 N. \quad (5)$$

We have checked numerically that the *average* shortest path between any two sites appears to increase logarithmically with system size  $N$  as well.

The networks HN3 and HN5 have the convenient but (from a mean-field perspective) unrealistic restriction of being planar. In fact, with a minor extension of the definition, it is easy to also design Hanoi networks that are

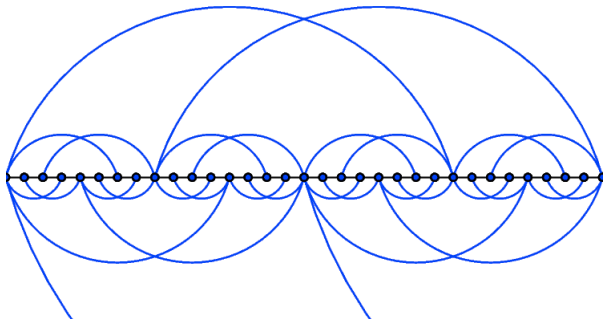


FIG. 3: (Color Online) Depiction of the non-planar Hanoi network HN3. Again, starting from a  $1d$ -backbone (black lines), a set of long-range bonds (blue-shaded lines) is added that break planarity but maintain the hierarchical pattern set out in Eq. (1). The RG on this network remains exact. Note that sites on the lowest two levels of the hierarchy have degree 3, then degree 5, 7, etc, comprising a fraction of  $1/2$ ,  $1/4$ ,  $1/8$ , etc., of all sites, which makes for an average degree of 4 in this network.

both, non-planar *and* fully renormalizable. The simplest such network, which we dub HN3, is depicted in Fig. 3.

To obtain the average degree, we observe that  $1/2 + 1/4$  of all sites have degree 3,  $1/8$  has degree 5,  $1/16$  has degree 7, and so on, leading to an exponentially falling degree distribution, as for HN5. The total number of bonds  $L$  in the system of size  $N = 2^k$  is

$$\begin{aligned} 2L &= 3 \times 2^{k-1} + \sum_{i=2}^{k-1} (2i-1) 2^{k-i} + 2k + (2k-2), \\ &= 4 \times 2^k - 4, \end{aligned} \quad (6)$$

and thus, the average degree is

$$\langle \alpha \rangle = \frac{2L}{N} \sim 4. \quad (7)$$

Here, too, it is easy to see that the shortest paths between sites increases logarithmically with system size  $N$ . Note that in the same manner we extended HN3 to HN5 by connecting even-indexed sites within each hierarchy, we will discuss such an extension of HN3 toward a non-planar network of average degree 6, HN6, in Sec. IV B.

### III. RG FOR THE ISING MODEL

In this section, we study Ising spin models on HN3, HN5 and HN3 with the renormalization group (RG) [6]. First, we consider RG for the Ising model on HN3. This allows us to introduce our procedure although the result turns out to be trivial in the sense that there is no finite-temperature transition. Especially, it is actually identical (except for one bond-type) to the exact RG for HN5, and it is almost identical to the treatment below for HN3.

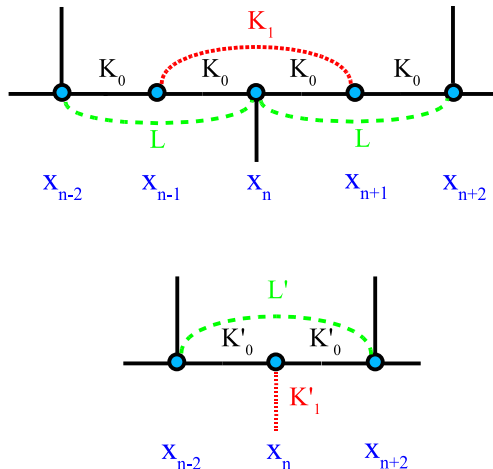


FIG. 4: (Color Online) Depiction of the (exact) RG step for the Ising model on HN3. The step consists of tracing out odd-labeled variables  $x_{n\pm 1}$  in the top plot and expressing the renormalized couplings ( $L'_0, K'_0$ ) on the bottom in terms of the old couplings ( $L_0, K_0, K_1$ ). Note that the original network in Fig. 1 does not contain couplings of type ( $L_0, L'_0$ ), but that they certainly become relevant during the process.

#### A. Ising Ferromagnet on HN3

The RG consists of recursively tracing out spins level-by-level in the hierarchy [12]. In terms of Eq. (1), we start by tracing out all sites with  $n$  odd, i.e.  $i = 0$ , then those  $n$  which are divisible by 2 only once, i.e.  $i = 1$ , and so on. We can always relabel all sites  $n$  after any RG step by  $n \rightarrow n/2$ , so that we trace out the respective odd-labeled sites at any level. It is apparent, for instance from Fig. 1, that odd-labeled sites are connected to their even-labeled nearest neighbors on the backbone, say, by a coupling  $K_0 (= \beta J_0)$ . At any level, each odd-labeled site  $x_{n\pm 1}$  is also connected to one other such site  $x_{n\mp 1}$  across an even-labeled site  $x_n$  with  $n = 2(2j+1)$  that is exactly *once* divisible by 2. Let us call that coupling  $K_1 (= \beta J_1)$ . The basic RG step is depicted in Fig. 4 and consists of tracing out the two sites  $x_{n\pm 1}$  neighboring the site  $x_n$  for all  $j$  with  $n = 2(2j+1)$ .

We can section the Ising Hamiltonian

$$-\beta\mathcal{H} = \sum_{n=1}^{2^{k-2}} (-\beta\mathcal{H}_n) + \mathcal{R}(K_2, K_3, \dots), \quad (8)$$

where  $\mathcal{R}$  contains all coupling terms of higher level in the hierarchy, and each sectional Hamiltonian is given by

$$\begin{aligned} -\beta\mathcal{H}_n &= 4I + L_0(x_{n-2}x_n + x_nx_{n+2}) + \\ &K_0(x_{n-2}x_{n-1} + x_{n-1}x_n + x_nx_{n+1} + x_{n+1}x_{n+2}) \\ &+ K_1x_{n-1}x_{n+1}, \end{aligned} \quad (9)$$

where  $(K_0, K_1, L_0)$  are the unrenormalized couplings defined in Fig. 4 and  $I$  is a constant that fixes the overall

energy scale per spin. (There are effectively 4 spins involved in each graph-let, as those at each boundary are equally shared with neighboring graph-lets.) While couplings of the type  $L_0$  between next-nearest even-labeled neighbors emerges that are not part of the network initially in HN3, they do emerge during the RG step (otherwise the system of recursion equations would not close), see Fig. 4.

To simplify the analysis, we introduce new variables similar to inverse “activities” [6],

$$C = e^{-4I}, \quad \kappa = e^{-4K_0}, \quad \lambda = e^{-4L_0}, \quad \mu = e^{-2K_1}, \quad (10)$$

which ensure that the RG flow only contains algebraic functions and, for the ferromagnetic model, remains confined within the physical domain  $0 \leq \kappa, \lambda, \mu \leq 1$ . Thus, we rewrite Eq. (9) as

$$e^{-\beta\mathcal{H}_n} = C^{-1} \kappa^{-\frac{1}{4}(x_{n-2}x_{n-1}+x_{n-1}x_n+x_nx_{n+1}+x_{n+1}x_{n+2})} \lambda^{-\frac{1}{4}(x_{n-2}x_n+x_nx_{n+2})} \mu^{-\frac{1}{2}x_{n-1}x_{n+1}}. \quad (11)$$

Tracing out the odd-labeled spins, we have to evaluate

$$\begin{aligned} & \sum_{\{x_{n-1}=\pm 1\}} \sum_{\{x_{n+1}=\pm 1\}} e^{-\beta\mathcal{H}_n} \\ &= C^{-1} \mu^{-\frac{1}{2}} \lambda^{-\frac{1}{4}(x_{n-2}x_n+x_nx_{n+2})} \\ & \quad \left[ \kappa^{-\frac{1}{4}(x_{n-2}+2x_n+x_{n+2})} + \mu\kappa^{-\frac{1}{4}(x_{n-2}-x_{n+2})} \right. \\ & \quad \left. + \mu\kappa^{\frac{1}{4}(x_{n-2}-x_{n+2})} + \kappa^{\frac{1}{4}(x_{n-2}+2x_n+x_{n+2})} \right] \\ &= (C')^{-\frac{1}{2}} (\lambda')^{-\frac{1}{4}x_{n-2}x_{n+2}} (\kappa')^{-\frac{1}{4}(x_{n-2}x_n+x_nx_{n+2})} \end{aligned} \quad (12)$$

for the remaining spins in terms of the *renormalized* quantities  $C', \kappa', \lambda'$ . Of the eight possible relations resulting from the combinations  $x_{n-2}, x_n, x_{n+2} = \pm 1$ , only three are independent. After some algebra, we extract from those the RG recursions:

$$\begin{aligned} \kappa' &= \kappa\lambda \frac{2(1+\mu)}{1+2\mu\kappa+\kappa^2}, \\ \lambda' &= \frac{(1+\kappa)^2(1+\mu)}{2(1+2\mu\kappa+\kappa^2)}, \\ C' &= C^2 \frac{\kappa\mu}{\sqrt{2}(1+\kappa)(1+\mu)^{\frac{3}{2}}\sqrt{1+2\mu\kappa+\kappa^2}}. \end{aligned} \quad (13)$$

Note that for couplings in higher levels of the hierarchy it is  $K'_i = K_{i+1}$  for  $i \geq 1$ ; correspondingly, these couplings, and hence,  $\mu$ , will *not* renormalize. Instead, they retain their “bare” value  $\mu^2$  determined by the temperature,  $kT/J = -2/\ln \mu$ . In this sense, we will use  $\mu$  as a measure of temperature throughout.

Only half of the contribution to the renormalized energy scale is originating with the sectional Hamiltonian in Eq. (9), since at the next level *two* such sections are combined into one, making  $C' \propto C^2$ . While we do not consider the recursions for  $C$  in this paper, they are essential to reconstruct the free energy for each system, and will be analyzed elsewhere [3].

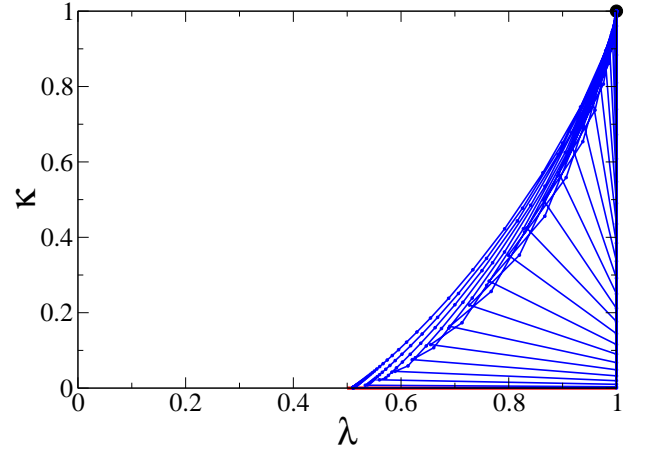


FIG. 5: (Color Online) Phase diagram for the Ising ferromagnet on HN3. The stable high-temperature fixed point at  $\kappa^* = \lambda^* = 1$  is marked by a black dot, the line of unstable fixed points at low temperature by a thick red line for  $\kappa^* = 0$  and  $\frac{1}{2} \leq \lambda^* \leq 1$ . For homogeneous initial conditions in Eq. (14), the ensuing RG flow for each  $\mu$  (blue lines) starts on the line  $\lambda^{(0)} = 1$  and evolves to a higher value of  $\kappa^{(1)}$  but smaller value of  $\lambda^{(1)}$  before it rapidly veers off toward the high-temperature fixed point. RG flow lines are drawn here for equal increments in  $\mu = \sqrt{\kappa^{(0)}}$ . Note that lines are allowed to cross, as each flow line is parameterized by a different value of  $\mu$ .

Eqs. (13) provide recursions order-by-order in the RG for the evolution of the effective couplings characterizing increasingly larger scales of the network. To facilitate this RG flow, we need to specify initial conditions for a particular physical situation realized in the unrenormalized, bare network. Here, we restrict ourselves to networks with uniform bonds (although many interesting choices are conceivable, such as distance-dependence [8, 23, 24]). For HN3 this implies that we chose  $J = 1$  as our energy scale, such that  $K_i = \beta J = \beta$  and  $I = L_0 = 0$  initially, or in terms of Eq. (10),

$$C^{(0)} = \lambda^{(0)} = 1, \quad \kappa^{(0)} = \mu^2 = e^{-4\beta}. \quad (14)$$

Searching for fixed points  $K'_0 = K_0 = K_0^*$  and  $L' = L = L^*$ , i.e.  $\kappa' = \kappa = \kappa^*$  and  $\lambda' = \lambda = \lambda^*$  in Eqs. (13), immediately provides the trivial, high-temperature solution  $\kappa^* = \lambda^* = 1$ , i.e.  $K_0^* = L^* = 0$ . Further analysis yields only a line of (unstable) strong-coupling fixed points,

$$\kappa^* = 0, \quad \lambda^* = \frac{1+\mu}{2}, \quad (15)$$

extending from  $\lambda^* = \frac{1}{2}$  for low temperatures,  $\mu = 0$ , to  $\lambda^* = 1$  for  $T \rightarrow \infty$ , where  $\mu = 1$ , see Fig. 5. Even at  $T = 0$ , only the renormalized backbone bonds  $K_0$  provide strong coupling, the emerging long-range bonds  $L_0$  only exert limited coupling strength.

Local analysis near the fixed points with the Ansatz

$$\kappa_n \sim \kappa^* + \epsilon_n, \quad \lambda_n \sim \lambda^* + \delta_n, \quad \epsilon_n, \delta_n \ll 1 \quad (16)$$

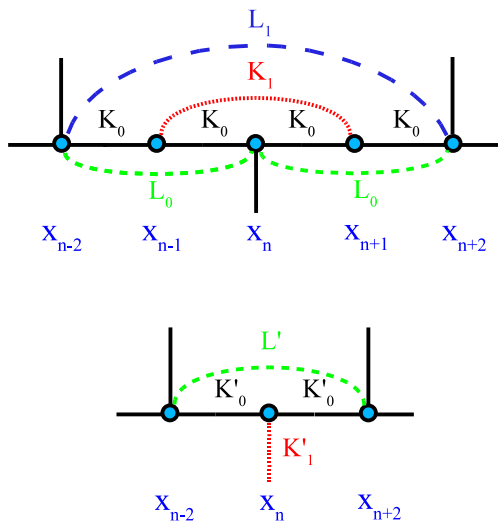


FIG. 6: (Color Online) Depiction of the (exact) RG step for the Ising model on HN5. This step is *identical* to that for HN3 in Fig. 4 aside from the extra link  $L_1$  spanning between  $x_{n-2}$  and  $x_{n+2}$  (top), which contributes to the renormalization of  $L'_0$  (bottom).

reveals that the high-temperature fixed point is always stable and corrections decay exponentially, where the exponential contains a factor of  $2^{\frac{2}{3}} = \sqrt{N}$ . At the low-temperature line of fixed points in Eq. (15) we find

$$\epsilon_n \sim \epsilon_0 (1 + \mu)^{2n}, \quad \delta_n \sim \frac{1 - \mu}{1 + \mu} \epsilon_0 (1 + \mu)^{2n}, \quad (17)$$

which is divergent for all  $T > 0$ , i.e.  $0 < \mu \leq 1$ , making the fixed point at  $T = 0$  unstable. For any fixed point, there is no linear expansion possible that would yield critical exponents. For the initial conditions in Eqs. (14) corresponding to uniform couplings throughout the unrenormalized network, the RG flow always evolves to the high-temperature fixed point, as Fig. 5 shows. Thus, the ferromagnet on this network behaves similar to a 1d Ising model.

### B. Ising Ferromagnet on HN5

As shown in Sec. II, HN5 is basically an extension of HN3, created by adding a new layer of links to each level of the hierarchy. As is apparent from the foregoing discussion in Sec. III A, these additions correspond precisely to new renormalizable operators (here, the bonds  $L$ ) that *inevitably emerge* during the RG of HN3, see Fig. 4. In HN5, these new operators are simply deemed an original feature of the network, hence, maintaining the RG as an exact procedure. Consequently, the RG itself hardly changes, see Fig. 6; it merely differs by one extra link in the graph-let,  $L_1$ , compared to that for HN3 in Fig. 4. In Eq. (9), it only adds the term  $L_1 x_{n-2} x_{n+2}$  to the sectional Hamiltonian and, like  $L_0$  itself,  $L_1$  does

not get traced over in the calculation in Eq. (12). We can introduce these new bonds as yet another free, non-renormalizing coupling in the RG and choose, to wit,

$$L_1 = yK_1, \quad \text{i.e.} \quad e^{-4L_1} = \mu^{2y}. \quad (18)$$

This merely contributes a factor of  $\mu^{-\frac{y}{4}x_{n-2}x_{n+2}}$  to the unprimed side of Eq. (12), which correspondingly alters only the recursion for  $\lambda'$  in Eq. (13) by a factor of  $\mu^{2y}$ . Otherwise using the same definitions as in Sec. III A, we obtain the RG recursions for the Ising ferromagnet on HN5:[32]

$$\begin{aligned} \kappa' &= \kappa \lambda \frac{2(1 + \mu)}{1 + 2\mu\kappa + \kappa^2}, \\ \lambda' &= \mu^{2y} \frac{(1 + \kappa)^2 (1 + \mu)}{2(1 + 2\mu\kappa + \kappa^2)}, \\ C' &= C^2 \frac{\kappa\mu}{\sqrt{2}(1 + \kappa)(1 + \mu)^{\frac{3}{2}} \sqrt{1 + 2\mu\kappa + \kappa^2}}. \end{aligned} \quad (19)$$

Accordingly, due to the bare existence of the  $L_1$  bond, we will have to change the initial conditions from Eq. (14) to

$$C^{(0)} = 1, \quad \kappa^{(0)} = \mu^2 = e^{-4\beta}, \quad \lambda^{(0)} = \mu^{2y}. \quad (20)$$

Analyzing these recursions for fixed points,  $\kappa' = \kappa = \kappa^*$  and  $\lambda' = \lambda = \lambda^*$ , we find that the addition of the extra long-range bond has *eliminated* the high-temperature fixed point found in HN3. At low temperatures, we find similar to Eq. (15) in HN3 a line of fixed points

$$\kappa^* = 0, \quad \lambda^* = \frac{\mu^{2y}}{2} (1 + \mu), \quad (21)$$

which here extends over the entire domain for the long-range bonds,  $0 \leq \lambda^* \leq 1$  for  $0 \leq \mu \leq 1$ . Note that although  $y$  represents a continuous interpolation between HN3 and HN5, there is a singular limit at  $y \rightarrow 0$  toward an isolated point corresponding to HN3, see Eqs. (15). In the following, we only treat the case of couplings that are homogeneous throughout the unrenormalized network,  $y = 1$ . Consideration of the rich set of transitions occurring for the family of networks parameterized by interpolating  $0 < y \leq 1$  is deferred to Sec. IV.

Dividing out the  $\kappa^* = 0$ -solution, further analysis of Eqs. (19) for  $y = 1$  reveals yet another line of fixed points given by

$$\begin{aligned} \kappa^* &= \frac{1}{2} \left[ -(1 - \mu)\mu + \sqrt{(1 + \mu)(\mu^3 - 3\mu^2 + 8\mu - 4)} \right], \\ \lambda^* &= \frac{\mu}{4} \left[ 2 - \mu + \mu^2 + \sqrt{(1 + \mu)(\mu^3 - 3\mu^2 + 8\mu - 4)} \right], \end{aligned} \quad (22)$$

which can be expressed most simply in closed form as

$$\lambda^* = \frac{1}{2} \left[ \kappa^* - 1 + \sqrt{5 + 2\kappa^* + 5(\kappa^*)^2 + 4(\kappa^*)^3} \right] \quad (23)$$

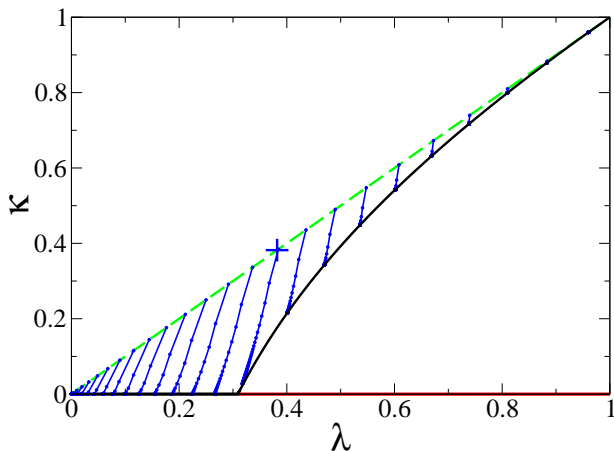


FIG. 7: (Color Online)Phase diagram for the Ising ferromagnet on HN5 with homogeneous bonds,  $y = 1$ . Unlike for HN3 in Fig. 5, there is no high-temperature fixed point here, instead a line of stable fixed points marked by a thick black line that extends from the strong-coupling regime at  $\kappa^* = 0$  and  $0 \leq \lambda^* < \frac{1}{2\phi} = 0.309017\dots$  all the way to the high-temperature regime. For the homogeneous-coupling initial conditions in Eq. (20), the ensuing RG flow (blue-shaded lines) starts on the diagonal (dashed line) and always evolves toward lower values of  $\kappa^*$  and  $\lambda^*$ . In the low-temperature regime, the flow reaches strong coupling,  $\kappa^* = 0$ , for values below  $\mu_c = \phi^{-1} = 0.618033\dots$  (cross at  $\kappa^{(0)} = \lambda^{(0)} = \mu_c^2$ ). Above that, the flow terminates on the line of finite-coupling fixed points, all the way to infinite temperature,  $\mu \rightarrow 1$ .

by eliminating  $\mu$ . As we will see, these relations lead to physical fixed points only within a limited range of the temperature  $\mu$ . We have plotted the phase diagram for HN5 at  $y = 1$  in Fig. 7. It also shows the RG flow for the initial conditions in Eqs. (20), which starts on the diagonal, representing all-equal bonds for the homogeneous network. For these initial conditions, the flow always evolves toward smaller values of  $\kappa$  and  $\lambda$ , i.e. stronger coupling. But there is a notable transition where the attained fixed point jumps from the low-temperature branch in Eq. (21) characterized by  $\kappa^* = 0$ , i.e. a solidly frozen backbone, to the branch given Eq. (23) on which both  $\kappa^*$  and  $\lambda^*$  are finite. We obtain this transition point by evaluating Eqs. (22-23) for  $\kappa^* = 0$ , which yields  $\lambda^* = \frac{1}{2\phi} = 0.309017\dots$  and a critical temperature of

$$\mu_c = \frac{1}{\phi}, \text{ or } \frac{kT_c}{J} = -\frac{2}{\ln \mu_c} = 4.156173842\dots, \quad (24)$$

where  $\phi = (\sqrt{5} + 1)/2 = 1.6180339887\dots$  is the “golden ratio” [13]. For bare couplings at this temperature, marked by a cross in Fig. 7, the RG flow marginally reaches the strong-coupling limit. In this network, for these initial conditions the RG flow never reaches an unstable fixed point such as the unstable portion of Eq. (21), marked by a red-shaded line in Fig. 7. As we will see below, this circumstance will change when we weaken the impact of long-range couplings.

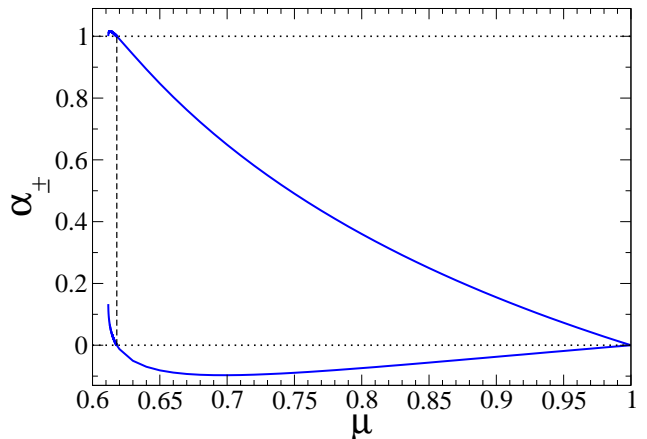


FIG. 8: (Color Online)Plot of the two eigenvalues  $\alpha_{\pm}$  (blue-shaded lines) resulting from Eq. (26). In the physical regime,  $\frac{1}{\phi} < \mu \leq 1$ , marked left by the vertical dashed line, both eigenvalues satisfy  $1 > \alpha_+ \geq 0 \geq \alpha_- > -1$ . Just below that regime,  $\alpha_+$  exceeds unity, re-enters, and both eigenvalues soon (at  $\mu = 0.6117\dots$ ) separately disappear into the complex plane.

### 1. Fixed-Point Stability

We determine the stability of the fixed points with a local analysis using Eq. (16). At  $y = 1$ , inserted into the strong-coupling solution, Eq. (21), provides

$$\epsilon_{n+1} = \mu^2 (1 + \mu)^2 \epsilon_n \quad (25)$$

and  $\delta_n \propto \epsilon_n$ . Thus, this line of fixed points is stable only for  $\mu$  smaller than the solution of  $1 = \mu(1 + \mu)$ , i.e.  $0 \leq \mu < \phi^{-1}$ ; for larger values of  $\mu$  the line is unstable. In terms of  $\lambda^*$ , this implies that the stability of the line of strong coupling fixed points changes exactly at the location in the phase diagram, Fig. 7, where the line of high-temperature fixed points in Eq. (23) intersects, at  $(\frac{1}{2\phi}, 0)$ . Applying the Ansatz on the line of high-temperature fixed points in Eqs. (22) yields after some algebra

$$\begin{aligned} \epsilon_{n+1} &= -\frac{1}{2\mu} \left( 2 - \mu - \sqrt{\frac{\mu^3 - 3\mu^2 + 8\mu - 4}{1 + \mu}} \right) \epsilon_n \\ &\quad + \frac{2 - 3\mu - \mu^2 + \sqrt{(1 + \mu)(\mu^3 - 3\mu^2 + 8\mu - 4)}}{2(1 - \mu)\mu} \delta_n, \\ \delta_{n+1} &= \frac{\mu}{2} - \frac{1}{2} \sqrt{\frac{\mu^3 - 3\mu^2 + 8\mu - 4}{1 + \mu}} \epsilon_n. \end{aligned} \quad (26)$$

The two eigenvalues  $\alpha_{\pm}$  characterizing this system are easy to find but lead to messy algebraic expressions; instead of presenting them, we merely plot their values as a function of  $\mu$  in Fig. 8. It shows that instability and a delicate root-singularity (at  $\mu = 1 + \frac{1}{3} \sqrt[3]{6\sqrt{114} - 27} - 5/\sqrt[3]{6\sqrt{114} - 27} = 0.6117\dots$ ) lurk just outside the physical regime,  $\phi^{-1} < \mu \leq 1$ , yet inside of that regime the

eigenvalues both satisfy  $|\alpha_{\pm}| < 1$  and the entire line of fixed points remains stable.

## 2. Divergence of the Correlation Length at $T_c$

The effect of the critical point at  $\mu_c = \frac{1}{\phi}$  on the scaling behavior of the Ising model deserves special attention. For instance, we can associate a correlation length  $\xi$  at a given temperature  $\mu$  to the system by considering the approach to the stable fixed point, which is derived from the dominant eigenvalue  $\alpha_+(\mu) < 1$  of Eq. (26) affecting the asymptotic behavior of the backbone couplings  $\kappa_n$ ,

$$\epsilon_n \sim (\alpha_+)^n \epsilon_0 \sim e^{-\frac{n}{n^*}},$$

defining a cut-off scale  $n^*$ . Aside from a few initial transient rescalings, associated with local structure of the network, the appearance of the physical state of the system remains scale invariant,  $\epsilon_{n+1} \sim \epsilon_n$ , for system sizes  $N = 2^n$  with  $n < n^*$ . In turn, for larger systems with  $n > n^*$ , correlated domains of size

$$\xi(\mu) \sim 2^{n^*} = e^{-\frac{\ln 2}{\ln \alpha_+}} \quad (27)$$

become mutually decorrelated to attest to the off-critical macroscopic state of the system. Only for  $\mu \rightarrow \mu_c$  does the correlation length diverge: Expanding the eigenvalue resulting from Eqs. (26) for  $\mu \rightarrow \mu_c^+$ , we obtain  $\alpha_+ \sim 1 - a(\mu - \mu_c)$  with  $a = 2\sqrt{5}$ . In fact, the corresponding expansion around the strong-coupling fixed point in Eq. (21) for  $\mu \rightarrow \mu_c^-$ , we obtain  $\alpha_+ \sim 1 - a(\mu_c - \mu)$  with the same constant  $a$ , so that we can write  $\alpha_+ \sim 1 - a|\mu - \mu_c|$  and get

$$\xi \sim e^{\frac{\ln 2}{a|\mu - \mu_c|}}, \quad \mu \rightarrow \mu_c. \quad (28)$$

This exponential divergence neither resembles the power-law divergence for a finite-order phase transition of Ising systems on a lattice nor the infinite-order transition characteristic of BKT that we discuss below.

## C. Ising Ferromagnet on HNNP

HNNP represents a drastic change in the geometric properties over the other Hanoi networks, HN3 and HN5, while nonetheless preserving the exact RG. Here, a crossing set of bonds  $K_1$  in the elementary graph-let shown in Fig. 9 render this network non-planar. Yet, its average degree of 4 is between that for HN3 and HN5, and we will see that the effective strength of the renormalized coupling is intermediate between HN3 and HN5, too: Unlike HN3, it does have an ordered low-temperature regime, but unlike for the transition in HN5, its high-temperature regime above  $T_c$  only possesses a high-temperature fixed point of vanishing coupling strength; not enough to sustain the partially ordered state found in HN5.

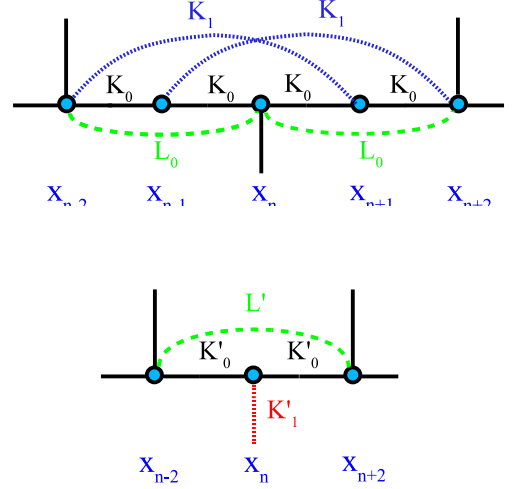


FIG. 9: (Color Online) Depiction of RG step for the Ising model on HNNP. This step differs from that for HN3 in Fig. 4 and HN5 in Fig. 6 as there are a set of crossing long-range bonds in each elementary graph-let before the RG step (left). But the resulting graph-let after the RG step is again identical to that for HN3 and HN5.

The structural feature of the crossing bonds is reflected in the Ising Hamiltonian, of course, and we find for its sectional Hamiltonian

$$-\beta\mathcal{H}_n = 4I + L_0(x_{n-2}x_n + x_nx_{n+2}) + K_0(x_{n-2}x_{n-1} + x_{n-1}x_n + x_nx_{n+1} + x_{n+1}x_{n+2}) + K_1(x_{n-2}x_{n+1} + x_{n-1}x_{n+2}) \quad (29)$$

Following the same procedure as in Eqs. (10-13) yields the RG recursions

$$\begin{aligned} \kappa' &= \kappa\lambda \frac{(1+\mu)^2}{(1+\mu\kappa)^2}, \\ \lambda' &= \frac{(\kappa+\mu)^2}{(1+\mu\kappa)^2}, \\ C' &= C^2 \frac{\kappa\mu^2}{(1+\mu)^2(\kappa+\mu)(1+\mu\kappa)}, \end{aligned} \quad (30)$$

with the same initial conditions as for HN3 in Eq. (14).

Once more inspecting these recursions for fixed points,  $\kappa' = \kappa = \kappa^*$  and  $\lambda' = \lambda = \lambda^*$ , we find a strong-coupling line of fixed points at

$$\kappa^* = 0, \quad \lambda^* = \mu^2, \quad (31)$$

which extends over the entire domain for the long-range bonds,  $0 \leq \lambda^* \leq 1$  for  $0 \leq \mu \leq 1$ . We can similarly identify a high-temperature fixed point at

$$\kappa^* = \lambda^* = 1 \quad (32)$$

that is valid for all  $\mu$ . Further analysis of Eqs. (30) reveals

yet another line of fixed points given by

$$\kappa^* = \frac{1 - \mu - \mu^2}{\mu^2}, \quad \lambda^* = \frac{(1 - \mu)^2}{\mu^2}. \quad (33)$$

It is clear that this line of fixed points is physical merely in the range  $\frac{1}{2} \leq \mu \leq \frac{1}{\phi}$  beyond which one or both of  $\kappa^*$  and  $\lambda^*$  leaves the unit interval. We can express this line in closed form,

$$\kappa^* = \lambda^* + \sqrt{\lambda^*} - 1, \quad (34)$$

by eliminating  $\mu$ .

We have plotted the phase diagram for HNNP in Fig. 10. It also shows the RG flow for the initial conditions in Eqs. (14), which starts on the right-hand vertical axis,  $\lambda^{(0)} = 1$ . For these initial conditions, there appears to be an ordinary, finite-order phase transition, with the RG-flow diverging from an unstable fixed point toward a solidly frozen ordered regime at lower temperatures and a plain disordered regime above. Yet, the transition is non-universal, for instance, dependent on the initial ratio between  $K_0$  and  $K_1$  bonds. There is no patchy order in this system, as there are apparently not enough long-range bonds to enforce it, compared to HN5. The actual critical temperature  $T_c$  is the transcendental solution of an infinite integration of the RG-recursions in Eq. (30) from the initial conditions in Eq. (14), which can be obtained to any accuracy by a shooting procedure. With that, we obtain

$$\mu_c = 0.553814426157623\dots, \quad (35)$$

or

$$T_c = -\frac{2}{\ln \mu_c} = 3.3845207164300986\dots, \quad (36)$$

marked by a blue cross in Fig. 10. Inserted into Eqs. (33), this places the unstable fixed point governing the critical behavior for these particular initial conditions at  $(\kappa^*, \lambda^*) = (0.4547454105\dots, 0.64908641578\dots)$ , labeled by a red dot.

### 1. Fixed-Point Stability

We explore the stability of these fixed points with a local analysis, using again the Ansatz in Eq. (16). First, we consider the strong-coupling fixed point in Eq. (31). Expanding the RG-recursion for  $\kappa'$  with the Ansatz yields

$$\epsilon_{n+1} = \mu^2 (1 + \mu)^2 \epsilon_n, \quad (37)$$

immediately proving that this fixed point is stable *only* for  $\mu < \frac{1}{\phi}$ , where the  $\kappa = 0$ -line intercepts with the other line of fixed points in Eqs. (33) or (34). For values above that,  $\kappa^* = 0$  becomes unstable. Conversely, expanding

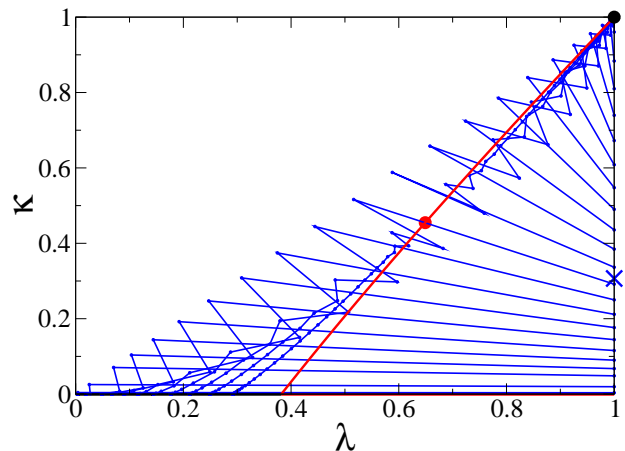


FIG. 10: (Color Online) Phase diagram for the Ising ferromagnet on HNNP. Similar to HN3 in Fig. 5, there is again a high-temperature fixed point here (black dot). Though, more akin to HN5 in Fig. 7, a line of fixed points extends along  $\kappa^* = 0$  and  $0 \leq \lambda^* \leq 1$ , which for  $\lambda^* < \phi^{-2}$  is stable (thick black line) and unstable above (thick red line). Both regimes are connected by a (red) line of unstable fixed points given by Eq. (34) with an intercept at  $\lambda = \phi^{-2} = 0.381966\dots$ . For the homogeneous-bond initial conditions in Eq. (14), the ensuing RG flow (blue lines) starts from  $\lambda^{(0)} = 1$ , evolves toward the diagonal  $\kappa^{(1)} = \lambda^{(1)}$  first, and proceeds in an oscillatory manner. For initial temperatures below the critical point  $\mu_c^2 = 0.30671\dots$  ( $\times$ ), the RG flow eventually veers toward strong coupling,  $\kappa^* = 0$ , and above, to the high-temperature fixed point. The particular fixed point governing the flow for these initial conditions is marked by a red dot.

around the high-temperature fixed point in Eq. (32) gives

$$\begin{aligned} \epsilon_{n+1} &= \frac{1 - \mu}{1 + \mu} \epsilon_n + \delta_n, \\ \delta_{n+1} &= \frac{2(1 - \mu)}{1 + \mu} \epsilon_n, \end{aligned} \quad (38)$$

which possesses the eigenvalues

$$\alpha_{\pm} = \frac{1 - \mu}{2(1 + \mu)} \left[ 1 \pm \sqrt{1 + 8 \frac{1 + \mu}{1 - \mu}} \right]. \quad (39)$$

The lower branch for all  $0 < \mu < 1$  remains confined to  $-1 < \alpha_- < 0$ , while  $1 < \alpha_+ < 2$  for  $\mu < \frac{1}{2}$ ; only for  $\mu > \frac{1}{2}$  is this fixed point stable. In the overlap,  $\frac{1}{2} < \mu < \frac{1}{\phi}$ , of the stable regimes of the two previous fixed points, we find the remaining line of fixed points in Eqs. (33), which prove to be unstable. To show that, we insert the Ansatz to obtain the system

$$\begin{aligned} \epsilon_{n+1} &= \frac{\mu^2 + 2\mu - 1}{1 - \mu^2} \epsilon_n + \frac{1 - \mu - \mu^2}{(1 - \mu)^2} \delta_n, \\ \delta_{n+1} &= \frac{2\mu}{1 + \mu} \epsilon_n. \end{aligned} \quad (40)$$



The eigenvalues  $\alpha_{\pm}$  of this system are given by

$$\alpha_{\pm} = \frac{\mu^2 + 2\mu - 1 \pm \sqrt{1 + 4\mu + 2\mu^2 - 12\mu^3 - 7\mu^4}}{2(1 - \mu^2)} \quad (41)$$

for which  $\alpha_+ > 1$  and  $0 > \alpha_- > -1$  on the physically relevant interval  $\frac{1}{2} < \mu < \frac{1}{\phi}$ . Thus, any fixed point on that line has an unstable direction and a stable but *oscillatory* direction, as is apparent for the flow in Fig. 10.

## 2. Divergence of the Correlation Length at $T_c$

Although we have found that the phase diagram for HNNP consists of lines of stable and unstable fixed points, only one specific unstable fixed point controls the scaling behavior for any specific incarnation of the system. Any such incarnation is selected by the initial choice of couplings  $(\kappa^{(0)}, \lambda^{(0)})$  as a function of temperature  $\mu$ . The controlling fixed point in Eq. (33) is a non-trivial consequence of these initial conditions. It is in particular a function of the specific critical temperature  $\mu_c$  for which it is reached. The induced scaling behavior for nearby temperatures is thus non-universal. Yet, for a given  $\mu_c$ , the local analysis for such an unstable fixed point proceeds identically to that for Ising systems on a lattice [6]. Here we have two scaling fields, whose fixed-point analysis leads to two eigenvalues in Eq. (41) that yields one relevant and one irrelevant variable. From the eigenvalue  $\alpha_+ (> 1)$  for the relevant variable, we obtain for the correlation-length exponent

$$\nu = \frac{1}{y_+} = \frac{\ln 2}{\ln \alpha_+(\mu_c)} \approx 10.8301 \dots, \quad (42)$$

such that

$$\xi \sim |\mu - \mu_c|^{-\nu}. \quad (43)$$

Thus, we find that the correlation length on approach to the fixed point merely diverges with a power law here. In this particular case, the exponent  $\nu$  happens to be very large, such that it would be difficult to distinguish this divergence from the exponential kind numerically.

## IV. INTERPOLATION BETWEEN HANOI NETWORKS

We have already observed in the construction of HN5 in Sec. III B that it is easy to promote the  $L$ -couplings, which inevitably emerge during the RG, to be associated with an actual bond in the network. Here, we will fully exploit this fact to obtain a one-parameter family of problems with various regimes of phase behaviors, based on the interpolating parameter  $y$  in Eq. (18). This procedure has also been used in Ref. [17] and a similar construction can already be found in Ref. [9]. In particular, we discover transitions between such regimes as a function of

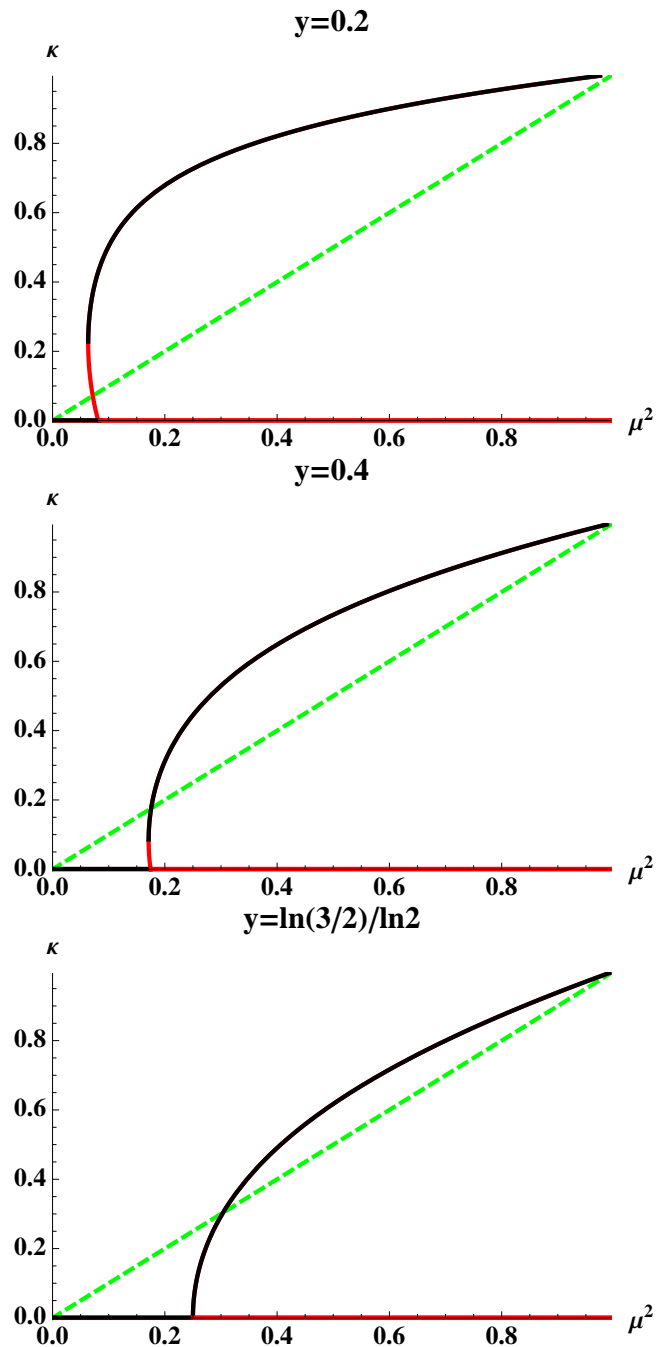


FIG. 11: (Color Online) Plot of  $\kappa^*$  in Eq. (44) as a function of  $\mu^2$  for  $y$  as defined in Eq. (18) for the interpolation between HN3 and HN5. The generic cases are represented by  $y = 0.2$  (top),  $y = 0.4$  (middle), and the special value of  $y = \frac{\ln(3/2)}{\ln 2} = 0.58 \dots$  (bottom) at which the branch point (BP) “sunset” out of the physical regime and the behavior becomes similar to that for  $y = 1$  shown in Fig. 7. In all cases, the dashed line indicates the initial conditions (IC) for the RG flow in Eqs. (19-20),  $\kappa^{(0)} = \mu^2$ . For  $\mu$  fixed, the RG flow *must* proceed vertically, either up or down, to the nearest stable line of fixed points. For low  $y$  (top), the IC cross the unstable branch below BP which then can *not* be reached by the flow. Once the IC cross above BP (middle), the flow *must* pass BP, unless BP sunsets (bottom).

the parameter that will allow us to clarify the connections between the diverse set of behaviors that we have discovered in the previous section.

### A. Interpolation between HN3 and HN5

In Sec. III B, we argued for the introduction of small-world bonds with couplings  $L_i$  and developed the RG recursions in (19) assuming a relative strength of these couplings to those germane to HN3 of the form in Eq. (18). Here, we will now consider the behavior that results from varying the strength parameter  $y$  between the two extremes already explored,  $y = 0$  for HN3 in Sec. III A and  $y = 1$  for HN5 in Sec. III B.

Inspecting these recursions in Eq. (19) for fixed points, we already found the low-temperature fixed point line in Eq. (21). Aside from this  $\kappa^* = 0$ -solution, Eqs. (19) further reveal a line of fixed points given by

$$\kappa^* = \frac{1}{2} \left[ \mu^y (1 + \mu) - 2\mu \pm \sqrt{\mathcal{D}_y(\mu)} \right], \quad (44)$$

$$\lambda^* = \frac{\mu^y}{4} \left[ 2(1 - \mu) + \mu^y (1 + \mu) \pm \sqrt{\mathcal{D}_y(\mu)} \right],$$

abbreviating the discriminant

$$\mathcal{D}_y(\mu) = (1 + \mu) [\mu^{2y} (1 + \mu) - 4(1 - \mu^y)(1 - \mu)]. \quad (45)$$

For  $y \rightarrow 0$ , this solution morphs into the high-temperature fixed point of HN3, see Fig. 5. But for any finite  $y$ , these lines of fixed points are non-trivial functions of  $\mu$ , as depicted for  $\kappa^*(\mu^2)$  in Fig. 11. The dominant feature in these plots is the root-singularity in  $\kappa^*$  with a branch point separating the upper stable and lower unstable line of fixed points. Essentially, three distinct generic regimes can be discerned: (1) If the branch-point happens to lie below the physical regime, we observe a phase transition without access to any unstable point (see bottom of Fig. 11); a critical point akin to that for HN5 at  $y = 1$  in Sec. III B arises. If the branch point rises into the physical regime, here for  $y < y_c = \frac{\ln(3/2)}{\ln 2} = 0.584963\dots$ , then depending on whether the initial conditions of the RG flow cross the critical line below or above the branch point, we find (2) a transition seemingly of finite-order on intercepting the unstable lower branch (see top of Fig. 11) for which the RG flow never accesses the branch point singularity. If, in turn, the initial conditions cross above, (3) a BKT-like transition results because the RG flow now *must* pass the singularity (see middle of Fig. 11), as we will show below.

#### 1. Fixed-Point Stability

As before, we determine the stability of the fixed points with a local analysis using Eq. (16). Inserting the Ansatz

for the strong-coupling solution, Eq. (21), yields

$$\epsilon_{n+1} = \mu^{2y} (1 + \mu)^2 \epsilon_n \quad (46)$$

and  $\delta_n \propto \epsilon_n$ . Thus, this line of fixed points is stable only for  $\mu$  smaller than the solution of  $1 = \mu^y (1 + \mu)$ ; for larger values the line is unstable. In each plot of Fig. 11, that value of  $\mu$  corresponds to the location on the  $\kappa = 0$ -line where the non-trivial fixed-point line intercepts.

Applying the Ansatz on the line of high-temperature fixed points in Eqs.(44) obtains now

$$\begin{aligned} \epsilon_{n+1} &= \frac{(1 + \mu) (\mu^y - 2) \pm \sqrt{\mathcal{D}_y(\mu)}}{2(1 + \mu) \mu^y} \epsilon_n \\ &+ \frac{2(1 - \mu) - \mu^y (1 + \mu) \pm \sqrt{\mathcal{D}_y(\mu)}}{2(1 - \mu) \mu^y} \delta_n, \\ \delta_{n+1} &= \frac{(1 + \mu) \mu^y \mp \sqrt{\mathcal{D}_y(\mu)}}{2(1 + \mu)} \epsilon_n. \end{aligned} \quad (47)$$

It is tedious but straightforward to show that the two eigenvalues  $\alpha_{1,2}$  characterizing this system indicate an upper stable branch for “+” and a lower unstable branch for “-”. Yet, the decisive question for the observed phase transition concerns the intercept with the initial conditions of the RG flow, i.e. the relative strengths of bare couplings in the network. If the intercept lies below the branch-point singularity, the phase transition is similar to that discussed in Sec. III C, although here the high-temperature phase flows not into a single point but rather into a temperature-dependent line of couplings, similar to (but inverted from) BKT. Apparently, such temperature-dependent couplings in themselves do not imply an infinite-order transition.

In turn, once those initial conditions pass *above* the branch point, such as in the middle panel of Fig. 11, there is no stable fixed point above that and the flow has to move toward lower values of  $\kappa$  during the RG flow. Whether there is any intercept with the upper branch makes little difference to the generic case here, as the critical behavior is controlled now by the flow in the immediate neighborhood of the root-singularity where both branches pinch off. Only in this case do we obtain an infinite-order transition of the BKT type.

#### 2. Divergence of the Correlation Length at $T_c$

We have already considered the exponential divergence characteristic of HN5 for  $y > y_c$  for the special case  $y = 1$  in Sec. III B 2. Similarly, we have found in Sec. III C 2 that HNNP at  $y = 1$  has a critical point very much like that found for HN5 at small  $y > 0$ , aside from a difference in the high-temperature coupling. For both cases, shown in the bottom and top panel of Fig. 11, respectively, further analysis would not alter the qualitative behavior in the divergence of the correlation length  $\xi$ .

Therefore, we restrict ourselves here to the novel case where the RG flow must pass near the branch-point singularity for a given choice of initial conditions displayed

in the middle panel of Fig. 11 for HN5 with  $y$  just below  $y_c$ . As has been argued for a similar case in a scale-free version of the hierarchical lattice [8], for temperatures  $\mu$  approaching the critical temperature  $\mu_c$  ever closer from below, the flow spends an ever larger number of iterations near the singularity. This characteristic number of RG iterations  $n^*(\mu)$  diverges for  $\mu \rightarrow \mu_c^-$  and can be interpreted as a correlation measure, just as in Sec. III B 2. But unlike the  $n^* \sim 1/|\mu_c - \mu|$  scaling there, we find here that  $n^* \sim 1/\sqrt{|\mu_c - \mu|}$ , leading to the BKT-like transition also found in many other networks.

To derive  $n^*$ , we follow Ref. [8] in ignoring the transient number of RG steps that would take us from the initial conditions to the singularity. Instead, we imagine that our flow would start right at the singularity but with an infinitesimally small shift down in temperature,

$$\tau = \mu_c - \mu, \quad (48)$$

so as to dislodge the flow from what is a fixed point for  $\mu = \mu_c$ . The system then decorrelates, i.e. the RG flow escapes the singularity by a finite amount, for sizes  $N = 2^n$ , i.e. after  $n > n^*$  iterations of the RG.

As the transition is obtained right at the branch point, the critical temperature  $\mu_c$  derives from

$$\mathcal{D}_y(\mu_c) = 0 \quad (49)$$

in Eqs. (44-45). We define the critical-point couplings

$$\begin{bmatrix} \kappa_c \\ \lambda_c \end{bmatrix} = \begin{bmatrix} \kappa^*(\mu_c) \\ \lambda^*(\mu_c) \end{bmatrix} = \begin{bmatrix} -\mu_c + \frac{\mu_c^y}{2}(1 + \mu_c) \\ \frac{\mu_c^y}{2}(1 - \mu_c) + \frac{\mu_c^{2y}}{4}(1 + \mu_c) \end{bmatrix} \quad (50)$$

from Eq. (44). Such a phase transition only exists for both,  $\kappa_c$  and  $\lambda_c$ , in the physical regime and, hence, it disappears when  $\kappa_c = 0$  is reached. The simultaneous solution of  $\kappa_c = 0$  and Eq. (49) yield

$$y_c = \frac{\ln \frac{3}{2}}{\ln 2} \quad \text{at} \quad \mu_c = \frac{1}{2}, \quad (51)$$

see Fig. 11 (bottom), with a transition similar to that at  $y = 1$  for all  $y > y_c$ .

For  $y < y_c$ , we expand Eqs. (19) around the branch point to 2nd order in  $\epsilon_n, \delta_n$  with

$$\begin{bmatrix} \kappa_n \\ \lambda_n \end{bmatrix} = \begin{bmatrix} \kappa_c + \epsilon_n \\ \lambda_c + \delta_n \end{bmatrix}$$

and  $\epsilon_0 = \delta_0 = 0$ . Note that neither  $\kappa_c$  nor  $\lambda_c$  depend on  $\mu$ ; it is precisely the *explicit* appearance of  $\mu$  in Eqs. (19) that allows a further 1st-order expansion in  $\tau$  according to Eq. (48). For general  $y$ , the solutions of Eq. (49) are too messy to display the results, but the nature of the recursions is as follows:

$$\begin{aligned} \epsilon_{n+1} &\sim A\tau + B\epsilon_n + C\delta_n + D\epsilon_n^2 + E\epsilon_n\delta_n, \\ \delta_{n+1} &\sim F\tau + G\epsilon_n + H\epsilon_n^2, \end{aligned} \quad (52)$$

dropping terms cubic in  $\epsilon, \delta$  and any smaller terms in  $\tau$ . All coefficients are algebraic functions of  $\mu_c$  and  $y$ . The proper scaling field  $u_n$  for the impending analysis is identified by multiplying the  $\delta$ -equation by  $C$  and combining it with that of  $\epsilon$ :

$$\begin{aligned} u_{n+1} &= \epsilon_{n+1} + C\delta_{n+1}, \\ &\sim (A + CF)\tau + (B + CG)\epsilon_n + C\delta_n \\ &\quad + (D + CH)\epsilon_n^2 + E\epsilon_n\delta_n. \end{aligned} \quad (53)$$

The subtlety of this procedure reveals itself now in the fact that  $B + CG \equiv 1$  for any  $\mu_c$  and  $y$ , and we can write with some new (positive) coefficients

$$u_{n+1} - u_n \sim u'(n) \sim -P\tau - Qu_n^2,$$

using a continuum approach justified for large  $n$ . In the limit  $\tau \rightarrow 0$ , this equation describes a singular boundary layer problem easily analyzed with the techniques outlined in Ref. [28]. Instead, we note that the differential equation can be solved exactly to give (with  $u_0 = 0$ ):

$$u_n \sim -\sqrt{\frac{P}{Q}}\tau \tan\left(\sqrt{PQ}\tau n\right). \quad (54)$$

Thus, the solution exits the boundary layer near the branch point (moving down toward the strong-coupling fixed point) and becomes finite for  $\sqrt{PQ}\tau n^* \rightarrow \pi/2$ , and we identify the scaling

$$n^* \sim \frac{1}{\sqrt{\tau}} = \frac{1}{\sqrt{\mu_c - \mu}}, \quad (55)$$

which by Eq. (27) leads to the divergence in the correlation length characteristic of BKT,

$$\xi(\mu) \sim e^{\frac{\text{const}}{\sqrt{\mu_c - \mu}}}, \quad \mu \rightarrow \mu_c^-. \quad (56)$$

Clearly, the physical origin of this singularity is not even remotely related to an actual BKT transition. In fact, instead of its rarity, confined to very particular lattice models, we may find it to be one of a few generic types of transition in networks.

## B. Interpolation between HNNP and HN6

Similar to the step from HN3 to HN5, we can add the emerging bonds  $L_1$  again as an original feature of the network, which we parameterize as in Eq. (18). As a result, we obtain a network that has an average degree of 6 with an exponential distribution of bonds which we will call HN6, accordingly. While difficult to display, HN6 consists of the addition of the green-shaded bonds from HN5 in Fig. 2 to HNNP in Fig. 3.

As in Eq. (18), we add the extra  $L$ -bonds with an initial coupling strength that is a  $y$ -fraction of the original HNNP bonds; for  $y \rightarrow 0$  we approach the pure HNNP from before, and for  $y = 1$  we attain HN6 with all equal

couplings. In this calculation, we get similar to Eqs. (19)

and (30):

$$\begin{aligned}\kappa' &= \kappa\lambda \frac{(1+\mu)^2}{(1+\mu\kappa)^2}, \\ \lambda' &= \mu^{2y} \frac{(\kappa+\mu)^2}{(1+\mu\kappa)^2}, \\ C' &= C^2 \frac{\kappa\mu^2}{(1+\mu)^2(\kappa+\mu)(1+\mu\kappa)},\end{aligned}\quad (57)$$

which is a simple extension of Eqs. (30), to which these RG recursions reduce for  $y = 0$ . Similar to the interpolation between HN3 and HN5, this interpolation between HNNP and HN6 also possesses interesting phase behavior. In particular, we also find a non-trivial value of  $y_c$  separating a HNNP-like phase diagram for low  $y$  from one similar to HN5 for larger  $y$ .

First, we find from Eqs. (57) the strong-coupling fixed-point line

$$\kappa_0^* = 0, \quad \lambda_0^* = \mu^{2+2y}, \quad (58)$$

which is stable for all  $\mu$  below the solution of  $1 = \mu^{1+y}(1+\mu)$ . The remaining fixed points in the physical regime satisfy

$$\kappa^* = -\frac{1}{\mu} + \frac{1+\mu}{2\mu^{2-y}} \left[ 1 \pm \sqrt{\Delta_y(\mu)} \right], \quad (59)$$

$$\lambda^* = -\frac{1-\mu}{\mu^{1-y}} + \frac{1}{2\mu^{2-2y}} \left[ 1 \pm \sqrt{\Delta_y(\mu)} \right], \quad (60)$$

where we abbreviate the discriminant

$$\Delta_y(\mu) = 1 - 4\mu^{1-y}(1-\mu). \quad (61)$$

Note that for  $y \rightarrow 0$ , the upper branches condense into the high-temperature fixed point of HNNP,  $\kappa^* = \lambda^* \rightarrow 1$ , and the lower branch becomes the unstable fixed-point line of HNNP. It is similarly easy to show that, indeed, for all  $0 \leq y \leq 1$ , “+” corresponds to stable fixed points and “-” to unstable ones.

At this point, it is obvious that the behavior for this system parallels that for HN5 above. In Fig. 12, we display for representative values of  $y$  the dependence of  $\kappa^*$  in Eq. (59) as a function of temperature  $\mu$ , which in each panel is equivalent to those in Fig. 11: For the smallest values of  $y$  (here, including also  $y = 0$ ), the initial conditions in Eq. (14) result in an RG flow that avoids the branch-point singularity and instead cross a line of unstable fixed points, one of which dominates the critical behavior that leads to a non-universal power-law divergence in the correlation length  $\xi$  as in Eq. (43) for  $y = 0$ . For stronger long-range couplings in the network, beyond some value of  $y$  for those initial conditions, that intercept moves above the branch point, forcing the flow through it at the critical point, which now develops a BKT-like essential singularity in  $\xi$ . Increasing such coupling strength further moves the branch point below the physical regime, out of reach from any initial condition.

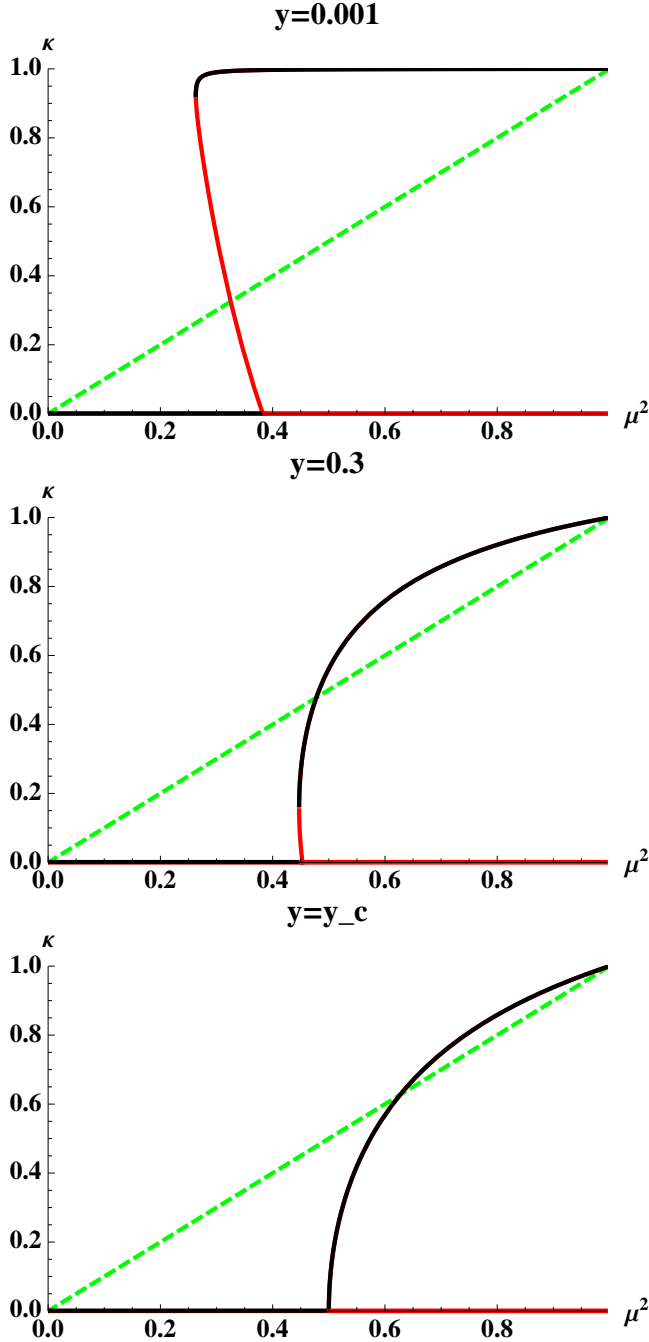


FIG. 12: (Color Online) Plot of  $\kappa^*$  in Eq. (59) as a function of  $\mu^2$  for  $y$  as defined in Eq. (18) for the interpolation between HNNP and HN6, similar to Fig. 11. The generic cases are represented by  $y \approx 0$  (top),  $y = 0.3$  (middle), and the special value of  $y = 2 \left[ \frac{\ln(1+\sqrt{2})}{\ln 2} - 1 \right] = 0.54\dots$  (bottom) at which the branch point “sunset” out of the physical regime, see discussion in Fig. 11.

Here, this requires both,  $\Delta_y(\mu)$  in Eq. (61) and  $\kappa^*$  in Eq. (59), to vanish, which occurs for

$$\begin{aligned}\mu_c &= \frac{1}{\sqrt{2}}, \\ y_c &= -\frac{\ln[\mu_c(1+\mu_c)]}{\ln\mu_c} = 0.5431066\dots\end{aligned}\quad (62)$$

Hence, for all  $y > y_c$ , there is no more high-temperature line of unstable fixed points and HN6 behaves identical to HN5 in Sec. III B.

The analysis of the critical behavior for the regimes of  $y_c < y \leq 1$  and for  $y$  just below  $y_c$  proceeds identically to Sec. III B and Sec. IV A, respectively. For the former, we just mention that the expansion along the upper stable branch obtains

$$\begin{aligned}\epsilon_{n+1} &= \frac{\mu^2 - \sqrt{\Delta_y(\mu)}}{1 - \mu^2} \epsilon_n \\ &\quad + \left[ \frac{\mu^{-y}}{1 - \mu} - \frac{\mu(1 - \sqrt{\Delta_y(\mu)})}{2(1 - \mu)^2} \right] \delta_n, \\ \delta_{n+1} &= \frac{\mu^y}{1 + \mu} \left[ 1 - \sqrt{\Delta_y(\mu)} \right] \epsilon_n.\end{aligned}\quad (63)$$

For example, at  $y = 1$ , the behavior of the eigenvalues  $\alpha_{\pm}$  of this system qualitatively resemble that in Fig. 8: The larger eigenvalue destabilizes (i.e. exceeds unity) when the temperature is lowered to

$$\mu_c = \frac{1}{3} \left[ \sqrt[3]{\frac{25 - 3\sqrt{69}}{2}} + \sqrt[3]{\frac{25 + 3\sqrt{69}}{2}} - 1 \right] = 0.754878\dots\quad (64)$$

or  $kT_c/J = 7.11239\dots$ , below which both eigenvalues disappear separately into the complex plane at  $\mu = \frac{3}{4}$ . Near  $\mu_c$ , we find for the dominant eigenvalue  $\alpha_+ \sim 1 - a|\mu - \mu_c|$ , with a constant  $a = \frac{2}{3} \left[ 1 + \sqrt[3]{(623 - 75\sqrt{69})/2} + \sqrt[3]{(623 + 75\sqrt{69})/2} \right] = 6.43855\dots$ , leading to the same conclusion as in Sec. III B 2 with a correlation length given by Eq. (28).

In turn, for values of  $y$  just below  $y_c$ , we locate the branch point via  $\Delta_y(\mu_c) = 0$  to obtain the critical temperature  $\mu_c(y)$  and find

$$\begin{bmatrix} \kappa_c \\ \lambda_c \end{bmatrix} = \begin{bmatrix} \kappa^*(\mu_c) \\ \lambda^*(\mu_c) \end{bmatrix} = \begin{bmatrix} \frac{1-2\mu_c^2}{\mu_c} \\ \frac{1-2\mu_c^2}{4\mu_c(1-\mu_c)^2} \end{bmatrix}, \quad (65)$$

where we have eliminated all explicit reference to  $y$ . Following the steps subsequent to Eq. (50), we find in the

same manner a BKT-like divergence of  $\xi$  as in Eq. (56).

## V. CONCLUSION

We have analyzed the fixed-point structure of an Ising ferromagnet on a set of Hanoi networks with an exact real-space renormalization group. Using interpolating families of such networks, with the relative coupling strength  $y$  between backbone and small-world bonds as the interpolation parameter, we reveal a number of regimes with distinct critical behaviors. While in each such regime the critical transition has non-universal features, the characteristics of the transition in each one has generic, robust features. For increasing strength, we observe that the divergence in the correlation length changes from power-law  $x^{-\nu}$ , to a BKT-like essential singularity  $e^{1/\sqrt{x}}$ , then to a plain essential singularity  $e^{1/x}$ , on approach to the critical point  $x \sim |\mu_c - \mu| \rightarrow 0$ . We trace the changes from one regime to the next in terms of the analytic structure of the RG flow. Finding an enumerable range of such characteristics hints at a possible classification of critical behavior of statistical models in networks generally, a task we will explore in more detail elsewhere [3]. For example, critical properties of the kind found here have also been observed in community formation [9] and in percolation [11, 16, 29–31]. The existence of entire regimes that exhibit essential singularities in the divergence of the correlations, as we have found here, might explain the surprising prevalence of typically quite rare BKT-like transitions in otherwise unrelated network models [2].

There are a number of possible extensions of this work, which we are currently exploring. Here, we have merely focused on the fixed-point structure and exclusively considered the divergence of the correlation length. We are currently developing the RG scheme to investigate more complicated observables to extract insights into the physical origin of these peculiar critical phenomena. Merely the addition of an external field as a generator for magnetic properties already makes the analysis much more complicated by breaking the  $Z_2$ -symmetry, thus allowing for yet another renormalizable bond linking three spins simultaneously [18]. As well, the study of other models spin in this context seems desirable. The absence of a bipartite structure (i.e. the existence of odd-length loops) in the Hanoi networks promises interesting effects due to frustration, which can be calculated with similar rigor for an anti-ferromagnetic system (and, at least, numerically exact for a spin glass). The results of those investigations are forthcoming.

[1] S. Boccaletti, V. Latora, Y. Moreno, M. Chavez, and D.-U. Hwang, Phys. Rep. **424**, 175 (2006).

[2] S. N. Dorogovtsev, A. V. Goltsev, and J. F. F. Mendes, Rev. Mod. Phys. **80**, 1275 (2008).

- [3] S. Boettcher and C. T. Brunson, (unpublished).
- [4] V. L. Berezinskii, Zh. Eksp. Teor. Fiz. **59**, 907 (1970).
- [5] J. M. Kosterlitz and D. Thouless, J. Phys. C **6**, 1181 (1973).
- [6] M. Plischke and B. Bergersen, *Equilibrium Statistical Physics, 2nd edition* (World Scientific, Singapore, 1994).
- [7] M. Bauer, S. Coulomb, and S. N. Dorogovtsev, Phys. Rev. Lett. **94**, 200602 (2005).
- [8] M. Hinczewski and A. N. Berker, Phys. Rev. E **73**, 066126 (2006).
- [9] M. Hinczewski, Phys. Rev. E **75**, 061104 (2007).
- [10] E. Khatjeh, S. N. Dorogovtsev, and J. F. F. Mendes, Phys. Rev. E **75**, 041112 (2007).
- [11] A. N. Berker, M. Hinczewski, and R. R. Netz, Phys. Rev. E **80**, 041118 (2009).
- [12] S. Boettcher, B. Goncalves, and H. Guclu, J. Phys. A: Math. Theor. **41**, 252001 (2008).
- [13] S. Boettcher and B. Goncalves, Europhys. Lett. **84**, 30002 (2008).
- [14] S. Boettcher, B. Goncalves, and J. Azaret, J. Phys. A: Math. Theor. **41**, 335003 (2008).
- [15] J. Otwinowski and S. Boettcher, Journal of Statistical Mechanics: Theory and Experiment **2009**, P07010 (2009).
- [16] S. Boettcher, J. L. Cook, and R. M. Ziff, Phys. Rev. E **80**, 041115 (2009).
- [17] S. Boettcher, C. Varghese, and M. A. Novotny, (arXiv:1011.6348).
- [18] S. Boettcher and A. K. Hartmann, (unpublished).
- [19] D. J. Watts and S. H. Strogatz, Nature **393**, 440 (1998).
- [20] A.-L. Barabasi and R. Albert, Science **286**, 509 (1999).
- [21] A.-L. Barabasi, *Linked: How Everything Is Connected to Everything Else and What It Means for Business, Science, and Everyday Life* (Plume Books, 2003).
- [22] M. Barthelemy, Physics Reports **499**, 1-101 (2011),
- [23] G. Kotliar, P. W. Anderson, and D. L. Stein, Phys. Rev. B **27**, R602 (1983).
- [24] H. G. Katzgraber and A. P. Young, Phys. Rev. B **67**, 134410 (2003).
- [25] A. N. Berker and S. Ostlund, J. Phys. C: Solid State Phys. **12**, 4961 (1979).
- [26] J. S. Andrade, H.-J. Herrmann, R. F. S. Andrade, and L. R. da Silva, Phys. Rev. Lett. **94**, 018702 (2005).
- [27] R. F. S. Andrade, J. J. S. Andrade, and H. J. Herrmann, Phys. Rev. E **79**, 036105 (2009).
- [28] C. M. Bender and S. A. Orszag, *Advanced Mathematical Methods for Scientists and Engineers* (McGraw-Hill, New York, 1978).
- [29] T. Nogawa and T. Hasegawa, J. Phys. A: Math. Theor. **42**, 145001 (2009).
- [30] T. Hasegawa, M. Sato, and K. Nemoto, Phys. Rev. E **82**, 046101 (2010).
- [31] T. Hasegawa, T. Nogawa, and K. Nemoto, ArXiv e-prints (2010), 1009.6009.
- [32] Absent the  $K_i$  bonds for  $i > 0$ , these relations trivially reproduce the  $1d$ -hierarchical lattice with small-world bonds.